

Near Field Radio-Frequency Electromagnetic Field Exposure of a Western Honey Bee

David Toribio, *Student Member, IEEE*, Wout Joseph, *Senior Member, IEEE*, and Arno Thielens, *Member, IEEE*

Abstract—It has been suggested that the wireless network evolution to smaller carrier wavelengths (from 2G to 5G) increases radio-frequency electromagnetic field (RF-EMF) absorption in Western Honey Bees (*Apis mellifera*). It is unknown whether the radiation performance of antennas is stable when an insect appears in their vicinity. In this research, the absorbed power in a worker honey bee and the influence of the bee's presence on antennas' radiation performance is investigated for the newly used frequencies in 5G networks, from 6-240 GHz. To these aims, numerical simulations using the finite-difference time-domain method were performed, in which a bee model, obtained by micro-CT scanning, was employed. These simulations showed that in the near field, the absorbed power can increase by a factor of 53, from 6-240 GHz. This is a factor of 7 higher than the increase reported in the far field, in previous studies. Furthermore, the simulations revealed that antennas' radiation efficiency can decrease by up to -40 % when a bee appears in the near field. Likewise, it was found that the gain pattern depends on the separation distance between the bee and the antenna, with a stronger dependency for higher frequencies.

Index Terms—Radio-frequency electromagnetic fields, RF-EMF exposure, near field, dipole antenna, western honey bees, millimeter waves, finite-difference time-domain method.

I. INTRODUCTION

WIRELESS telecommunication base stations are the dominant sources of outdoor radio-frequency electromagnetic fields (RF-EMFs) [1]. These RF-EMFs can be absorbed in dielectric media, and can cause dielectric heating [2]. Therefore, an RF-EMF exposure of sufficiently high intensity can cause thermal effects in all living organisms. These thermal effects of RF-EMF exposure have been shown for insects in [3]–[9], and have led to research on the RF-EMF absorption in insects [10], on the dielectric properties of insects [3], and on the use of RF-EMFs as an insect control method [4]–[6].

As telecommunication networks become more advanced, their frequency range is increasing from below 6 GHz (2G, 3G, 4G, and Wi-Fi) up to 300 GHz (5G). Therefore, part of their wavelengths of operation, the so-called millimeter-wavelengths, have become more comparable to the size of certain insects. It has been shown that this evolution to smaller carrier wavelengths could increase RF-EMF absorption in insects [10], [11].

RF-EMF absorption as a function of frequency was first reported in insects in [10], from 2-120 GHz, covering present and future telecommunication bands. This study showed that the

far-field RF-EMF absorption in insects is frequency dependent, and that it is maximized at wavelengths comparable to the insects's size. Research initiatives on RF-EMF exposure of insects have been concentrating on Western Honey Bees (*Apis mellifera*), because of their environmental and economical importance. Furthermore, RF dosimetry at 0.6-120 GHz in different developmental stages and castes of honey bees, and a coupling of this absorption to real RF-EMF exposure situation was investigated in [11]. This study confirmed the dependency of the far-field absorbed power in honey bees on the frequency and on the bee's size. In particular, this study revealed that the far-field absorbed power in honey bees increases with frequency up to 6-12 GHz, and that this absorbed power seems to maximize at a wavelength of about twice the longest dimension of the bee. Comparable frequency trends have been observed in humans [12], [13]. Moreover, in [11], it was shown that a small shift of 10 % of the incident power density to frequencies higher than 3 GHz could lead to an increase of the RF-EMF absorbed power in honey bees by a factor of 3. Such a shift is expected in future networks. The influence of low frequency magnetic fields on honey bees has been studied in [14], [15]. Potential effects of RF-EMF exposure on reproduction and behavior of honey bees were investigated in [16].

When an antenna is placed in the vicinity of a dielectric medium, electromagnetic contrast at the air/medium interface results in the appearance of scattered field and near field interactions, which modify the field in the medium [17], [18]. This coupling impacts the power absorption in the dielectric medium, as well as the resulting heating [19]. Moreover, these near field interactions, can significantly affect antenna characteristics such as the antenna reflection coefficient, radiation pattern and efficiency [20].

RF-EMF absorption by lossy media in the near field of antennas, and the effect of the near field coupling in the antenna characteristics have been investigated using human phantoms, at microwave and millimeter waves [21]–[23]. Due to the relatively small size of insects in comparison to the used carrier wavelengths in the current telecommunication networks, near field interactions between insects and antennas have not been explored up to now. However, in 5G networks with higher carrier frequencies, near field interactions might become more significant. This manuscript aims to explore such effects using *Apis mellifera*, as a model insect.

It would be relevant to investigate the RF-EMF exposure near (phased) arrays, since the base stations and user equipment of future telecom networks will contain antenna arrays [24]. However, at the moment, the only available

literature on RF-EMF exposure of insects studies far-field exposure [10], [11]. In order to make the transition to a study of an antenna array, it is first necessary to study the RF-EMF interactions near a single antenna element.

The goals of this paper are to study in the one hand, the near field frequency dependency of the absorbed power in a worker honey bee, for the newly used frequencies in 5G networks, from 6-240 GHz. Additionally, the influence of the bee's presence on the antennas' radiation performance is investigated. To this aim, numerical simulations are executed using standard dipole antennas that resonate in the targeted frequency band and a worker honey bee 3D model, obtained using micro-computerized tomography (CT) scanning. These results are important for legislators that are interested in environmental policy regarding RF-EMF exposure and for network operators that might be faced with insects appearing near their telecom antennas.

The main novelties and contributions of this paper are the numerical study of the near field RF-EMF exposure of an insect, for the first time. Moreover, this paper is the first to investigate the influence of the appearance of an insect in front of an antenna on its radiation characteristics.

II. METHODS

A. Studied honey bee, imaging technique and model development

Western Honey Bees are the most spread honey bee worldwide. A healthy honey bee colony can contain approximately 50,000 individuals. Most of these are sterile, female, worker bees. Worker bees perform all the tasks within a colony to keep it full of provisions and free from disease.

The worker bee used in this study is the same studied in [11]. It was scanned at the Western Sydney University National Imaging Facility (Sydney, Australia) using a bench-top Micro-CT scanner (Quantum GX MicroCT Imaging System, PerkinElmer, Hopkinton, MA, USA). No approval from a review board was needed for the scanning of an invertebrate. The bee had a full body length of approximately 11.0 mm long, was 5.0 mm wide and had a mass of approximately 900 mg.

The development of the 3D model of the bee is described in [11]. It involved the reconstruction of the projection images, using the software running on the Quantum GX, bench-top Micro-CT scanner. Then, the BeeView volume rendering software (DISECT Systems Ltd, Suffolk, UK) was used to acquire the bee's volume data from the image stack. The 3D model of the bee was created using the software TomoMask (www.tomomask.com), which generated a 3D model exported as an STL (STereo Lithography). The models were also smoothed using the Taubin $\frac{\lambda}{\mu}$ smoothing scheme [25], implemented in MeshLab [26]. The dimensions of the model and mesh integrity were checked (and corrected if necessary) before simulations using Netfabb (Autodesk, San Rafael, CA, USA).

B. Numerical simulations

Numerical simulations were executed to estimate RF-EMFs in and around a worker Western Honey Bee under near-

field exposure. These simulations were performed using the finite-difference time-domain (FDTD) method implemented in Sim4Life (ZMT, Zurich, Switzerland). This is a common technique used to determine RF-EMF in and near homogeneous and heterogeneous dielectric objects [10], [12], [27]. In this method, the simulation domain is divided in cubes using a three-dimensional rectilinear grid.

This time-domain technique requires a predefined simulation time (number of simulated periods), and a spatial grid step in order to reach a steady-state solution. These settings depend on the chosen spatial resolution, wavelength, size of the simulation, and feature sizes of the objects in the simulations. The FDTD algorithm requires a grid step smaller than one tenth of the smallest wavelength (λ) in the simulation domain in order to return stable solutions [28]. The smallest wavelength in tissue ($\frac{\lambda}{\sqrt{\epsilon_r}}$) is 1.1 mm at 120 GHz, and 0.56 mm at 240 GHz. Therefore, for frequencies in between 6-120 GHz, a grid step of 0.05 mm was used, whereas for 240 GHz, a grid step of 0.025 mm was used, with ϵ_r being the relative permittivity of the bee. Hence, in all simulations, a grid step less or equal than $0.045 \times \frac{\lambda}{\sqrt{\epsilon_r}}$, was used.

To investigate near field behavior as a function of frequency, numerical simulations at seven harmonic frequencies from 6-240 GHz (sinusoidal waves at a single frequency) were executed. The dielectric properties of the honey bee were quantified as conductivity (σ) and relative permittivity (ϵ_r). The dielectric properties of the honey bee were assigned using the same literature database and interpolation presented in [10]. The honey bee was modeled as an homogeneous object. This is an approximation, since real insects have heterogeneous tissue properties.

For the near-field exposure simulations, half wavelength dipole antennas, were designed to operate at the frequencies of interest, and with a power reflection coefficient ($|S_{11}|^2$) lower than -10 dB. Dipoles were selected because they are generic and relatively simple antennas that can, at a later stage, be fabricated in a laboratory setup. Table I shows the characteristics of these dipoles. The Fraunhofer far field distance is calculated as:

$$\frac{2 \times Dim^2}{\lambda} \quad (1)$$

where Dim represents either the largest dimension of the antenna (5th row of Table I), or the longest diagonal of the bounding box around the bee (6th row), see Fig. 1 for a reference to the bounding box and its diagonal. Thus, the far field distance for each antenna is the largest of the values in the 5th row and the 6th row of Table I.

The frequencies, grid steps, and dielectric properties, used in the simulations are listed in Table II. For each frequency, one simulation was performed for each of the 10 different relative separation distances (D), between the honey bee and the dipole employed in this research, for assessing the near field exposure of the honey bee. D ranged between $0.1 - 10\lambda$. D was limited to 10λ in order to keep simulations' size under dimensions supported by the simulation software.

Moreover, for each frequency studied, one far-field simulation was completed with a single-frequency sinusoidal

Characteristics	6 GHz	12 GHz	24 GHz	60 GHz	90 GHz	120 GHz	240 GHz
λ (mm)	50	25	12.5	5	3.3	2.5	1.3
d (mm)	1.6	0.8	0.4	0.2	0.1	0.03	0.03
L (mm)	10.6	5.3	2.6	1.05	0.8	0.5	0.3
g (mm)	0.12	0.6	0.3	0.01	0.008	0.003	0.003
Gain (dBi)	2.3	2.2	2.2	2.2	2.2	2.2	2.2
Fraunhofer distance (antenna)	0.4λ	0.4λ	0.4λ	0.4λ	0.4λ	0.4λ	0.4λ
Fraunhofer distance (bee)	0.1λ	0.5λ	2λ	12.3λ	27.8λ	49.4λ	197.8λ

Table I: Dipoles' characteristics. "d" refers to the diameter of the antenna's arms. "L" refers to the length of the antenna's arms. "g" refers to the gap between the antenna's arms. See Fig. 1 for a visual description of the antennas' dimensions.

(harmonic) continuous plane wave with a root-mean-squared electric field strength of 1 V/m, to compare between the far-field and near-field exposure of the honey bee. Therefore, the simulations' data set resulted in 7 (frequencies) \times 10 (separation distances) + 7 (plane waves) = 77 simulations.

Each simulation was implemented until a steady-state was reached. In the simulations in which the separation distance was between $0.1 - 3 \lambda$, the simulation duration was set to 10 simulated periods, while in simulations with separation distances of 7, 8 and 10λ , the duration was set to 30, 31 and 33 simulated periods, respectively. To validate that the simulations reached steady state in these number of simulated periods, the electric field strength along a line in the simulation domain was temporally monitored.

Properties	6 GHz	12 GHz	24 GHz	60 GHz	90 GHz	120 GHz	240 GHz
Maximum grid step	0.05 mm	0.025 mm					
ϵ_r	38	28.6	14.9	7	5.9	5.5	5
σ (S/m)	5.1	12	21.1	27.9	28.9	29.2	29.6

Table II: Simulations' settings and dielectric properties of the worker honey bee.

After each simulation, Sim4Life computes the internal electric field of the honey bee model, and uses it to calculate the total absorbed RF-EMF power (P'_{abs}) in the honey bee. P'_{abs} is calculated as the integrated product of the conductivity and the squared internal electric field strength over the total volume (V) of the honey bee:

$$P'_{abs} = \int_V \sigma \times |E_{int}^{\vec{r}}|^2 [W] \quad (2)$$

P'_{abs} is an important quantity since the dielectric heating of an insect is proportional to its absorbed RF-EMF power [2]. Then, in order to take into account the mismatch effect of the dipole due to the presence of the bee, P'_{abs} was normalized to the dipoles' accepted power. Thus, the results presented in this research are based on this normalized absorbed RF-EMF power (P_{abs}).

Also, in order to evaluate the incident power density due to the dipoles' radiation as an estimator of the bee's P_{abs} in the near field, the magnitude of the time-averaged Poynting vector $\langle \vec{S} \rangle$ was averaged over the frontal plane of the honey bee's bounding box. Sim4Life calculates the instantaneous Poynting vector (\vec{S}) at every voxel in the simulation domain as:

$$\vec{S} = \frac{1}{2} (\vec{E} \times \vec{H}^*) \left[\frac{W}{m^2} \right] \quad (3)$$

Therefore, $\langle \vec{S} \rangle$ at every voxel was calculated from the Sim4Life exported data as:

$$\langle \vec{S} \rangle = Re(\vec{S}) \left[\frac{W}{m^2} \right] \quad (4)$$

In the simulations in this research, the bee was placed in the \vec{z} direction, as depicted in Fig.1. Hence, an uncertainty study was conducted to quantify the influence on P_{abs} of placing the bee in the \vec{x} , \vec{y} , and diagonal directions. Furthermore, in the literature database of dielectric properties presented in [10], it was found that the largest deviations in dielectric properties between 6-240 GHz occur at 20 GHz, where ϵ_r can differ by +58% from the interpolated value, and σ can deviate by -32% from the interpolated value. Therefore, as part of the uncertainty study, 4 harmonic simulations at 24 GHz and $D = 0.8 \lambda$ were conducted, in which the dielectric properties assigned (see Table II) were altered in the following manner: $(1.6\epsilon_r, 1.4\sigma)$, $(1.6\epsilon_r, 0.6\sigma)$, $(0.4\epsilon_r, 1.4\sigma)$, $(0.4\epsilon_r, 0.6\sigma)$, therefore allowing for larger deviations than the estimated uncertainty on the chosen dielectric parameters.

Additionally, the influence of uncertainties in grid step and number of simulated periods on P_{abs} were evaluated. For this purpose, since variations in the two grid steps used in our simulations, 0.05 mm and 0.025 mm, should have the most influence in P_{abs} at 120 GHz and 240 GHz, respectively, one simulation at 120 GHz with a grid step of 0.025 mm, and another at 240 GHz with a grid step of 0.0125 mm were conducted, at $D = 0.8 \lambda$. Furthermore, 2 simulations at 240 GHz, one with $D = 3 \lambda$ and 40 simulated periods, and another with $D = 10 \lambda$ and 132 simulated periods were performed. Thus, the number of simulated periods in these simulations was 4 times higher than the originally assigned ones.

In order to assess the internal P_{abs} distribution in the bee, the internal electric field intensities normalized to the maximum internal electric field intensity $\left(\frac{|\vec{E}|}{|E_{max}|} \right)$ in a slice in the YZ plane at the center of the bee ($x = 0$ mm) was calculated, at each D and frequency. Moreover, the average of $\frac{|\vec{E}|}{|E_{max}|}$ in these slices as a function of D and frequency was determined.

III. RESULTS AND DISCUSSION

A. Antenna parameters as a function of separation distance

Fig. 2 shows that the maximum isotropic gain of the radiation pattern of each dipole decreases as the separation distance increases. This is attributed to the fact that as the bee is further away from the dipole, the near field coupling between the bee and the dipole weakens, and therefore, the dipoles' gain approaches their free space gain (2.2 dBi), as separation distance increases. However, the rate of this decrease is slower at higher frequencies (60 GHz, 90 GHz, 120 GHz, and 240 GHz) than at lower frequencies (6 GHz, 12 GHz, and 24 GHz). This occurs because 7λ is still not in the far field, when the dipoles operate at these higher frequencies.

Fig. 3 shows that as separation distance increases, the radiation efficiencies increase and approach a value of 1, at 7λ , at every frequency. Additionally, Fig. 3 shows that as frequency increases, the radiation efficiency decreases. This is

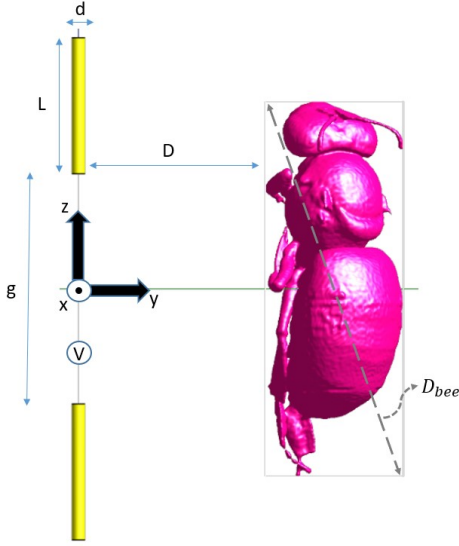


Figure 1: Dimensions and orientations of the dipoles and the bee. “D” is the separation distance between the dipole and the bee. “ D_{bee} ” is the diagonal of the smallest brick containing the bee phantom. “V” is the voltage source of the dipole. “d” is the diameter of the dipole’s arms. “L” is the length of the dipole’s arms. “g” is the gap between the dipole’s arms.

because the bee’s absorbed power decreases with increasing separation distances, and increases with increasing frequency, as will be demonstrated in Section III-C. Figs. 2 and 3 show that the presence of an insect in the near field of an antenna can influence the antenna’s radiation characteristics significantly. This impact can be more severe at higher frequencies.

The simulations also showed small fluctuations of the accepted power, and of the mismatch efficiency of the dipoles as a result of the near field coupling effects on the dipoles’ impedance. These coupling effects decrease as separation distance increases and disappear, in every frequency, once the bee is at a separation distance of 3λ . The maximal deviation from the 3λ stable value observed in accepted power and mismatch efficiency, were of 4% and 5%, respectively, at 24 GHz, at 0.1λ . Since the simulations showed highest deviations from the 3λ stable value at 12 and 24 GHz, it is assumed that these deviations are maximized at wavelengths that are most comparable with D_{bee} (see first row of Table III, see also Section III-D).

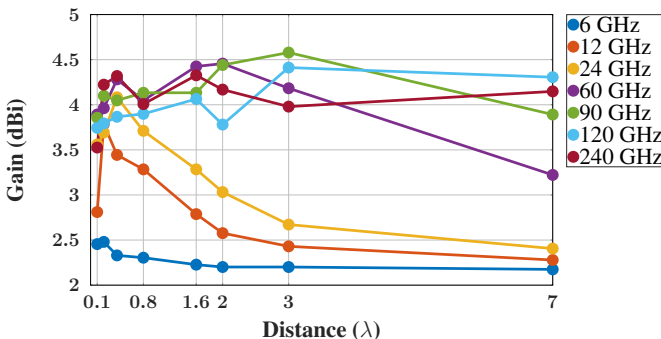


Figure 2: Maximum isotropic gain as a function of separation distance

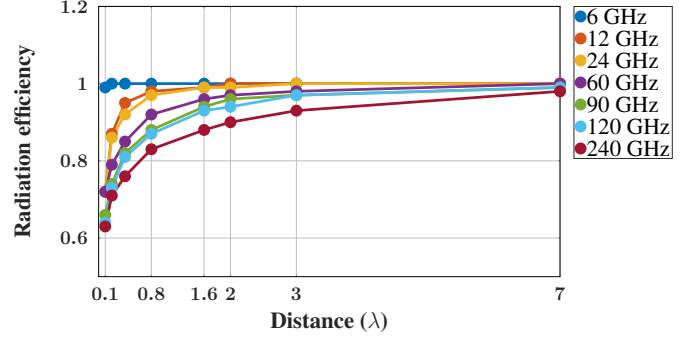


Figure 3: Radiation efficiency as a function of separation distance

	6 GHz	12 GHz	24 GHz	60 GHz	90 GHz	120 GHz	240 GHz
$\frac{D_{bee}}{\lambda}$	0.3	0.5	1	2.5	3.8	5	9.6
$P_{0,dB}$	-20.2	-5.6	-5.5	-5.5	-4.8	-4.5	-4.5
n	-2	-1.8	-1.5	-1	-0.8	-0.7	-0.6
δ_z (dB)	4.9	3.3	2.9	2.7	1.8	1.5	1.3

Table III: Dimension of bee in comparison to λ and path loss model parameters.

B. Gain as a function of separation distance and frequency

Simulation results showed that the gain, in the direction where the bee is located ($\phi = 90^\circ$), becomes more dependent on the separation distance as frequency increases. For instance, Fig. 4 shows that, at 60 GHz, when the bee is closer to the far field ($D = 3\lambda$), the gain is similar to the free space gain, however, as the bee approaches the dipole ($D = 0.1\lambda$), the gain in the direction that the bee approaches ($\phi = 90^\circ, \theta = 90^\circ$) decreases by a factor of 12 relative to the free space gain. Furthermore, the simulations revealed that the gain at $\phi = 90^\circ$ and $\theta = 0^\circ$ has a decreasing trend as D increases in all frequencies studied. This is due to an increase of energy reflection by the bee, in the $\theta = 0^\circ$ direction, as the bee gets closer to the dipole.

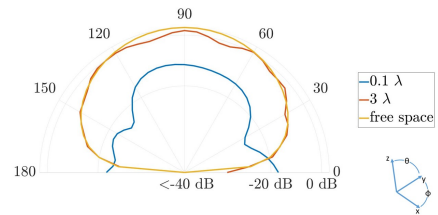


Figure 4: Dipole’s gain pattern as a function of D and θ , at $\phi = 90^\circ$, at 60 GHz.

C. Absorbed power as a function of separation distance and frequency

To model the bee’s absorbed power as a function of D, the following semi-empirical formula, expressed in decibel and based on the log-distance path loss model was used [29]:

$$P_{dB}(D) = P_{0,dB} + 10 \log \frac{D}{D_0} + X(\mu = 0, \sigma_X) \quad (5)$$

where D is the separation distance between the bee and the dipole, $P_{0,dB}$ is the bee's absorbed power in dB at the reference distance $D_0 = 0.1 \lambda$, n is the path loss exponent which equals -2 in free space, and X is a Gaussian variable with zero mean and variance σ_X^2 . Table III lists the parameter values of the fitted path loss model according to Equation (5), and the mean deviation of the measured results from the model (δ_z).

Fig. 5(a) shows that in the near field, the bee's absorbed power normalized to the accepted power (P_{abs}) decreases with increasing D , and increases with increasing frequency, when D is expressed as a factor of λ .

Figures 5(a) and 5(b) show that P_{abs} in the bee increases as a function of frequency, while in the far field a local maximum was found for P_{abs} as a function of frequency. This effect can be explained by an interplay between two factors: on the one hand, the power density that is incident on the bee increases with frequency for a fixed separation distance in terms of λ , which corresponds to a decreasing separation distance in absolute values, and on the other hand, a resonance effect that determines the efficiency of the absorption in the bee with maximum around 12 GHz. These two effects taken together result in the curves shown in Fig. 5(a) and the blue curve shown in Fig. 5(b).

Also, Fig. 5(b) shows that in the near field, at 0.2λ , P_{abs} increases 17.2 dB (a factor of 53) as frequency increases from 6-240 GHz, while in the far field, P_{abs} increases 4.4 dB (a factor of 2.77). Therefore, this figure shows that the near field increase in P_{abs} can be a factor of 19 higher than its far field increase, as a function of frequency. Additionally, this near field increase in P_{abs} is a factor of 7 higher than the increase in the far field, from 6-120 GHz, reported in [11]. The increase in P_{abs} under real exposure conditions is expected to be even more drastic, since currently most of the exposure is below 2 GHz, where P_{abs} should be even lower than at 6 GHz.

D. Comparison between near-field dipole and far-field plane wave simulations

Fig. 6 shows that the bee's P_{abs} normalized to $|\langle \vec{S} \rangle|$, averaged over the frontal plane of the honey bee's bounding box due to the dipoles' radiation approaches the normalized P_{abs} due to the plane waves, in the range of $3 - 10 \lambda$, at 6, 12 and 24 GHz.

Fig. 6 shows that, in contrast to the far field, in the near field, $|\langle \vec{S} \rangle|$ cannot be used as a proxy for the bee's P_{abs} , since in the near field, $|\langle \vec{S} \rangle|$ decreases at a faster rate than P_{abs} with increasing separation D , which explains the increasing trend of the $\frac{P_{abs}}{|\langle \vec{S} \rangle|}$ curve due to the dipoles' radiation as a function of D . For instance, it was found that when comparing the values at 0.1λ and 2λ , the ratios $\frac{|\langle \vec{S} \rangle(2 \lambda)|}{|\langle \vec{S} \rangle(0.1 \lambda)|}$ were 3 dB, 0.8 dB, and 0.5 dB lower than the ratios $\frac{P_{abs}(2 \lambda)}{P_{abs}(0.1 \lambda)}$ at 6, 12 and 24 GHz, respectively. Therefore, in the near field, $|\langle \vec{S} \rangle|$ can underestimate the bee's P_{abs} . This is in agreement with the results presented in [30].

It was found in [30] that using the modulus of the Poynting vector reduces the underestimation of the transmitted power

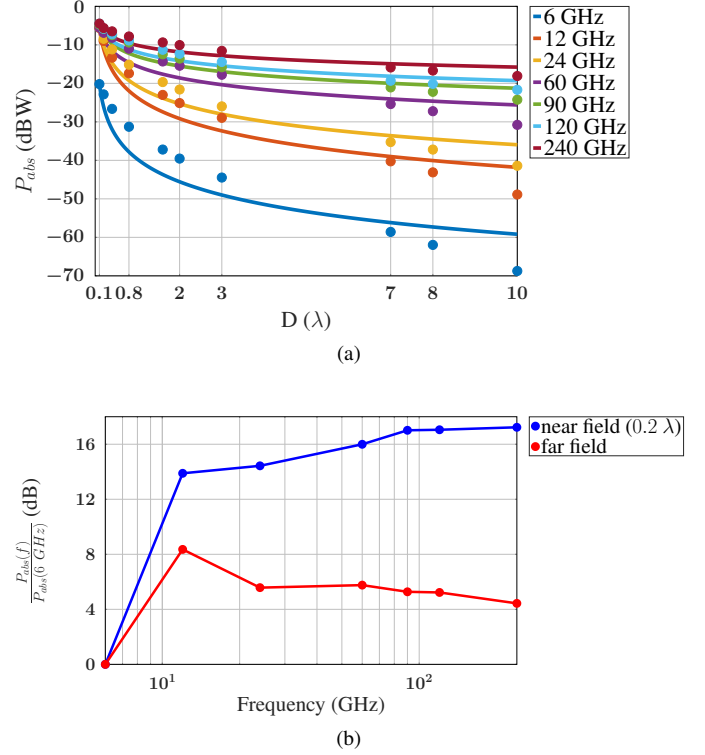


Figure 5: (a) Absorbed power as a function of D and frequency. Markers represent the values extracted from the simulations. The solid lines represent the fit according to the model of Equation (5). (b) Absorbed power in the near field ($D = 0.2 \lambda$) and in the far field, normalized to the absorbed power at 6 GHz, as a function of frequency.

density, in the near field of a planar body phantom. Hence, it would be relevant in our future research to evaluate and quantify if using the modulus of the Poynting vector can also reduce the underestimation of the whole-body averaged absorbed power, in the near field of insect phantoms.

Moreover, Fig. 6 shows that $\frac{P_{abs}}{|\langle \vec{S} \rangle|}$ maximizes at 12 GHz, and decreases as frequency increases beyond 12 GHz. This is in agreement with the results presented in [11] where it was observed that in the far field there is a resonance at 12 GHz, since at this frequency, the wavelength is about twice the longest dimension of the bee. In addition, this can be explained by a decrease in skin depth, driven by an increase in conductivity as frequency increases (see Table II and Section III-E).

E. Bee's internal electric field

The simulation results in Fig. 7 show that $\frac{|\vec{E}|}{|E_{max}|}$ in the bee are maximized at 12 GHz, and decrease with increasing frequency beyond 12 GHz. For instance, it was found that average $\frac{|\vec{E}|}{|E_{max}|}$ at 12 GHz are 14.6 dB higher than at 90 GHz, and 28.9 dB higher than at 240 GHz, at 0.2λ . In addition, Fig. 7 shows that as frequency increases above 12 GHz, $\frac{|\vec{E}|}{|E_{max}|}$ becomes more confined to the surface of the bee. This is attributed to the fact that the efficiency of RF-EMF coupling into the models is maximized at 12 GHz (see Section III-D).

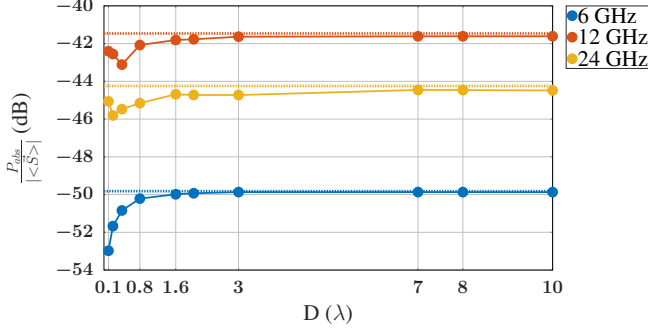


Figure 6: Absorbed power normalized to the magnitude of the time-averaged Poynting vector averaged over the frontal plane of the honey bee's bounding box relative to $1 \frac{W}{m^2}$ for an accepted power of 1 W. Solid lines: absorbed power due to dipoles' radiation. Dashed lines: absorbed power due to plane wave.

Since there is a direct proportionality between $\frac{|\vec{E}|}{|E_{max}|}$ and P_{abs} , it can be deduced that the fraction of incident power density, internally absorbed, is maximized at 12 GHz. This is the reason for the higher $\frac{P_{abs}}{|\langle \vec{S} \rangle|}$, at 12 GHz, in Fig. 6.

Furthermore, simulation results showed that for frequencies below 12 GHz, the average $\frac{|\vec{E}|}{|E_{max}|}$ remains constant across separation distances, whereas for frequencies higher than 12 GHz, the average $\frac{|\vec{E}|}{|E_{max}|}$ increases with increasing separation distance (D). Table IV shows a comparison of the average $\frac{|\vec{E}|}{|E_{max}|}$ at $D = 0.2 \lambda$ and at $D = 2 \lambda$. From these results, it can be concluded that the absorption cross section (ACS) which is an effective area of the bee, quantifying its efficiency in terms of power density absorption [31], increases with D, in frequencies above 12 GHz. On the other hand, the ACS remains constant for frequencies below 12 GHz. Hence, since $P_{abs} = ACS \times |\langle \vec{S} \rangle|$, the path loss exponent at frequencies below 12 GHz is lower, and closer to the path loss exponent of $|\langle \vec{S} \rangle|$ in free space. In contrast, at frequencies above 12 GHz, the increasing ACS with increasing D leads to a higher path loss exponent, as shown in Table III.

	6 GHz	12 GHz	24 GHz	60 GHz	90 GHz	120 GHz	240 GHz
$\langle \frac{ \vec{E} _{0.2\lambda}}{ E_{max} _{0.2\lambda}} \rangle$ (dB)	-23.3	-23.1	-24	-31.7	-37.7	-40.4	-52
$\langle \frac{ \vec{E} _{2\lambda}}{ E_{max} _{2\lambda}} \rangle$ (dB)	-23.7	-23.9	-23.4	-21.2	-24.3	-25.8	-31.8
$\Delta \langle \frac{ \vec{E} }{ E_{max} } \rangle$ (dB)	-0.4	-0.2	0.6	10.5	13.4	14.6	20.2

Table IV: Average $\frac{|\vec{E}|}{|E_{max}|}$ as a function of frequency and D. Second row: average $\frac{|\vec{E}|}{|E_{max}|}$, at $D = 0.2 \lambda$. Third row: average $\frac{|\vec{E}|}{|E_{max}|}$, at $D = 2 \lambda$. Fourth row: difference between third and second row.

F. Uncertainties

The percentage change in P_{abs} observed in the simulations, at 24 GHz and $D = 0.8 \lambda$, with altered dielectric properties of $(1.6\epsilon_r, 1.4\sigma)$, $(1.6\epsilon_r, 0.6\sigma)$, $(0.4\epsilon_r, 1.4\sigma)$, and $(0.4\epsilon_r, 0.6\sigma)$, is of 3%, 7%, -2.2%, and -11.2%, respectively. Additionally, it was noticed that changing the bee orientation to the \vec{x} direction, \vec{y} direction, and diagonal direction contributes to a maximal change in P_{abs} of -83.9%, as presented in Table V. Also, reducing the grid step by half at 120 GHz (to 0.025mm),

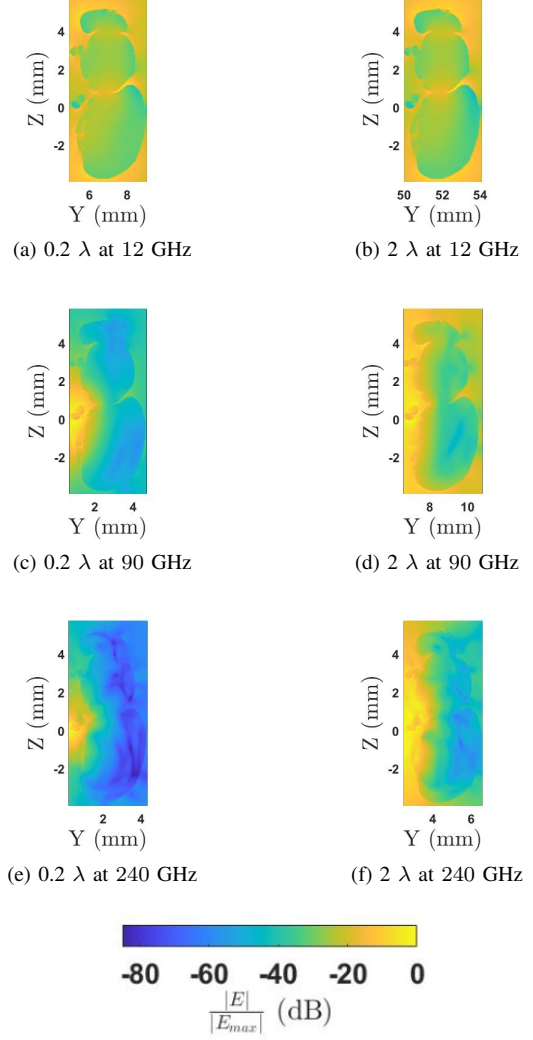


Figure 7: Bee's internal electric field intensities

and at 240 GHz (to 0.0125mm), leads to a change in P_{abs} of 1.3%, and 2.8%, respectively. These deviations produced by uncertainties in dielectric properties, bee orientation, and grid step are significant, but are much smaller than the factor of 53 increase in P_{abs} noticed from increasing the frequency from 6-240 GHz. Moreover, increasing the amount of simulated periods by a factor of 4, to 40 simulated periods, at 240 GHz and $D = 3 \lambda$, and to 132 periods, at 240 GHz and $D = 10 \lambda$ resulted in a change in P_{abs} of 0.01% and < 0.01%, respectively, which shows that the amount of simulated periods used in the simulations is sufficient.

Orientation	6 GHz	12 GHz	24 GHz	60 GHz	90 GHz	120 GHz	240 GHz
\vec{x}	-82.8%	-74.5%	-34.2%	-1.1%	20.3%	23.6%	31.9%
\vec{y}	-83.9%	-71.5%	-8.5%	-38.5%	-44.5%	-46.1%	-41.2%
Diagonal	-33.2%	-25.4%	-19.5%	-1.4%	13.2%	14.7%	15.9%

Table V: Percentage change in P_{abs} due to variation in bee orientation relative to the P_{abs} when the bee is \vec{z} oriented.

IV. CONCLUSION

Numerical simulations using finite-difference time-domain analysis were executed to calculate the radio-frequency electromagnetic fields (RF-EMFs) in and around a worker Western Honey Bee (*Apis mellifera*). This led to the quantification of the whole-body averaged absorbed radio-frequency power P_{abs} , under near-field exposure, in the frequency range of 6-240 GHz. The simulations showed that, in the near field, P_{abs} decreases as the separation distance between the bee and the dipole increases, and increases as frequency increases. The frequency behavior of P_{abs} in the near field is thus different to its far-field behavior, since, for a given accepted power and distance, in the near field P_{abs} increases with frequency (an average of 30.5 dB from 6-240 GHz), while in the far field P_{abs} in the worker bee is maximized at 12 GHz. This near-field increase in P_{abs} as a function of frequency, can be a factor of 7 higher than the far-field increase.

Moreover, these simulations allowed the study of the influence of the bee's position ($0.1 - 10 \lambda$ from the dipoles) in the radiation performance of the dipoles. In particular, it was found that as the separation distance increases, the dipoles' isotropic gain decreases and approaches their free-space gain. Also, it was noted that as a result of the near-field frequency behavior of P_{abs} , the dipoles' radiation efficiency decreases with increasing frequency and increases with increasing separation distance. Additionally, it was acknowledged that the gain pattern in the direction where the bee approaches the antenna depends on the separation distance between the bee and the antenna, with a stronger dependency for higher frequencies. This is important for 5G telecommunication networks, because they rely on infrastructure (antennas) whose performance can be influenced by the presence of free-flying insects.

Future directions of this research project will include the experimental validation of the results from the simulations presented in this paper, by completing near-field RF-EMF exposure measurements of honey bees. Furthermore, the RF-EMF interactions between honey bees and phased arrays will be investigated, since these are the type of antennas being deployed in high-frequency telecommunication networks. Additionally, we aim to investigate the thermal increase in the bee due to near field and far-field RF-EMF exposure, as a function of frequency, for instance, by means of infrared temperature measurements. Moreover, future work will also consist of performing simulations with heterogeneous honey bee phantoms, with tissue-specific dielectric properties.

ACKNOWLEDGMENT

Arno Thielens is a postdoctoral fellow of the Research Foundation Flanders (FWO) under grant agreement no. 12U1417N. This work was funded by the FWO under grant agreement no. G033220N. We would like to acknowledge Mark K. Greco, from the Medical Imaging unit at Charles Sturt University, NSW, Australia, for scanning the honey bee model.

REFERENCES

- [1] C. R. Bhatt, A. Thielens, B. Billah, M. Redmayne, M. J. Abramson, M. R. Sim, R. Vermeulen, L. Martens, W. Joseph, and G. Benke, "Assessment of personal exposure from radiofrequency-electromagnetic fields in Australia and Belgium using on-body calibrated exposimeters," *Environmental research*, vol. 151, pp. 547–563, 2016.
- [2] I. C. on Non-Ionizing Radiation Protection *et al.*, "Guidelines for limiting exposure to time-varying electric, magnetic, and electromagnetic fields (up to 300 GHz)," *Health physics*, vol. 74, no. 4, pp. 494–522, 1998.
- [3] S. O. Nelson, "Review and assessment of radio-frequency and microwave energy for stored-grain insect control," *Transactions of the ASAE*, vol. 39, no. 4, pp. 1475–1484, 1996.
- [4] S. Wang, J. Tang, R. Cavalieri, and D. Davis, "Differential heating of insects in dried nuts and fruits associated with radio frequency and microwave treatments," *Transactions of the ASAE*, vol. 46, no. 4, p. 1175, 2003.
- [5] B. Shrestha, D. Yu, and O.-D. Baik, "Elimination of *Cryptolestes ferrugineus* in wheat by radio frequency dielectric heating at different moisture contents," *Progress In Electromagnetics Research*, vol. 139, pp. 517–538, 2013.
- [6] N. Shayesteh and N. Barthakur, "Mortality and behaviour of two stored-product insect species during microwave irradiation," *Journal of Stored Products Research*, vol. 32, no. 3, pp. 239–246, 1996.
- [7] R. G. Olsen, "Insect teratogenesis in a standing-wave irradiation system," *Radio Science*, vol. 12, no. 6S, pp. 199–207, 1977.
- [8] E. Atli and H. Ünlü, "The effects of microwave frequency electromagnetic fields on the development of *Drosophila melanogaster*," *International journal of radiation biology*, vol. 82, no. 6, pp. 435–441, 2006.
- [9] J. H. Graham, D. Fletcher, J. Tigue, and M. McDonald, "Growth and developmental stability of *Drosophila melanogaster* in low frequency magnetic fields," *Bioelectromagnetics: Journal of the Bioelectromagnetics Society, The Society for Physical Regulation in Biology and Medicine, The European Bioelectromagnetics Association*, vol. 21, no. 6, pp. 465–472, 2000.
- [10] A. Thielens, D. Bell, D. B. Mortimore, M. K. Greco, L. Martens, and W. Joseph, "Exposure of insects to radio-frequency electromagnetic fields from 2 to 120 GHz," *Scientific reports*, vol. 8, no. 1, pp. 1–10, 2018.
- [11] A. Thielens, M. K. Greco, L. Verloock, L. Martens, and W. Joseph, "Radio-frequency electromagnetic field exposure of western honey bees," *Scientific Reports*, vol. 10, no. 1, pp. 1–14, 2020.
- [12] J. Bakker, M. Paulides, A. Christ, N. Kuster, and G. Van Rhoon, "Assessment of induced SAR in children exposed to electromagnetic plane waves between 10 MHz and 5.6 GHz," *Physics in Medicine & Biology*, vol. 55, no. 11, p. 3115, 2010.
- [13] A. Hirata, S. Kodera, J. Wang, and O. Fujiwara, "Dominant factors influencing whole-body average SAR due to far-field exposure in whole-body resonance frequency and GHz regions," *Bioelectromagnetics: Journal of the Bioelectromagnetics Society, The Society for Physical Regulation in Biology and Medicine, The European Bioelectromagnetics Association*, vol. 28, no. 6, pp. 484–487, 2007.
- [14] V. P. Bindokas, J. R. Gauger, and B. Greenberg, "Laboratory investigations of the electrical characteristics of honey bees and their exposure to intense electric fields," *Bioelectromagnetics: Journal of the Bioelectromagnetics Society, The Society for Physical Regulation in Biology and Medicine, The European Bioelectromagnetics Association*, vol. 10, no. 1, pp. 1–12, 1989.
- [15] T. E. Ferrari, "Magnets, magnetic field fluctuations and geomagnetic disturbances impair the homing ability of honey bees (*Apis mellifera*)," *Journal of Apicultural Research*, vol. 53, no. 4, pp. 452–465, 2014.
- [16] R. Odemer and F. Odemer, "Effects of radiofrequency electromagnetic radiation (RF-EMF) on honey bee queen development and mating success," *Science of The Total Environment*, vol. 661, pp. 553–562, 2019.
- [17] B. Derat, A. Cozza, and J.-C. Bolomey, "Influence of source-phantom multiple interactions on the field transmitted in a flat phantom," in *2007 18th International Zurich Symposium on Electromagnetic Compatibility*. IEEE, 2007, pp. 139–142.
- [18] B. Derat and A. Cozza, "Analysis of the transmitted field amplitude and SAR modification due to mobile terminal flat phantom multiple interactions," 2007.
- [19] T. Nakae, D. Funahashi, J. Higashiyama, T. Onishi, and A. Hirata, "Skin temperature elevation for incident power densities from dipole arrays at 28 GHz," *IEEE Access*, vol. 8, pp. 26 863–26 871, 2020.

- [20] A. R. Guraliuc, M. Zhadobov, R. Sauleau, L. Marnat, and L. Dussopt, "Near-field user exposure in forthcoming 5g scenarios in the 60 ghz band," *IEEE Transactions on Antennas and Propagation*, vol. 65, no. 12, pp. 6606–6615, 2017.
- [21] E. Reusens, W. Joseph, B. Latré, B. Braem, G. Vermeeren, E. Tanghe, L. Martens, I. Moerman, and C. Blondia, "Characterization of on-body communication channel and energy efficient topology design for wireless body area networks," *IEEE Transactions on Information Technology in Biomedicine*, vol. 13, no. 6, pp. 933–945, 2009.
- [22] N. Kuster and Q. Balzano, "Energy absorption mechanism by biological bodies in the near field of dipole antennas above 300 mhz," *IEEE Transactions on vehicular technology*, vol. 41, no. 1, pp. 17–23, 1992.
- [23] M. Ziane, R. Sauleau, and M. Zhadobov, "Antenna/body coupling in the near-field at 60 ghz: Impact on the absorbed power density," *Applied Sciences*, vol. 10, no. 21, p. 7392, 2020.
- [24] S. Shikhantsov, A. Thielens, G. Vermeeren, E. Tanghe, P. Demeester, L. Martens, G. Torfs, and W. Joseph, "Hybrid ray-tracing/fdtd method for human exposure evaluation of a massive mimo technology in an industrial indoor environment," *IEEE Access*, vol. 7, pp. 21 020–21 031, 2019.
- [25] G. Taubin, "A signal processing approach to fair surface design," in *Proceedings of the 22nd annual conference on Computer graphics and interactive techniques*, 1995, pp. 351–358.
- [26] P. Cignoni, M. Callieri, M. Corsini, M. Dellepiane, F. Ganovelli, and G. Ranzuglia, "Meshlab: an open-source mesh processing tool." in *Eurographics Italian chapter conference*, vol. 2008. Salerno, 2008, pp. 129–136.
- [27] G. Vermeeren, W. Joseph, and L. Martens, "Whole-body sar in spheroidal adult and child phantoms in realistic exposure environment," *Electronics Letters*, vol. 44, no. 13, pp. 790–791, 2008.
- [28] J. Hand, "Modelling the interaction of electromagnetic fields (10 mhz–10 ghz) with the human body: methods and applications," *Physics in Medicine & Biology*, vol. 53, no. 16, p. R243, 2008.
- [29] C. A. Balanis, *Antenna theory: analysis and design*. New York, Harper and Row, 1982.
- [30] A. Christ, T. Samaras, E. Neufeld, and N. Kuster, "Limitations of incident power density as a proxy for induced electromagnetic fields," *Bioelectromagnetics*, vol. 41, no. 5, pp. 348–359, 2020.
- [31] A. Bamba, W. Joseph, G. Vermeeren, A. Thielens, E. Tanghe, and L. Martens, "A formula for human average whole-body sarwb under diffuse fields exposure in the ghz region," *Physics in Medicine & Biology*, vol. 59, no. 23, p. 7435, 2014.



David Toribio (Student Member, IEEE) was born in Santo Domingo, Dominican Republic on 10 June, 1987. He received the M.Sc. degree in Electrical Engineering from Utah State University, Logan, UT, USA, in 2013, and the M.Sc. degree in Biomedical Engineering from The University of Miami, Coral Gables, FL, USA, in 2017. In July 2020, he joined the Waves Research Group in the Department of Information Technology, at Ghent University, Ghent, Belgium, where he is pursuing a Ph.D. degree in Electrical Engineering.

In 2009, he participated in the summer research undergraduate program at the Soft Tissue Bioengineering Laboratory at Purdue University, West Lafayette, IN, USA, where he studied wavelets de-noising techniques applied to cartilage magnetic resonance images. From 2018-2019, he was a research associate at the Cardiac Surgery Laboratory at the Katholieke Universiteit Leuven, where he worked in the design of a heart failure monitoring system. His current research focuses in the development of systems for electromagnetic entomology. In particular, he studies the RF-EMF interactions between insects and antennas, and designs systems for insects' tracking.



Wout Joseph (M'05) was born in Ostend, Belgium on October 21, 1977. He received the M. Sc. degree in electrical engineering from Ghent University (Belgium) in July 2000. He obtained the Ph. D. degree in March 2005; this work dealt with measuring and modelling of electromagnetic fields around base stations for mobile communications related to the health effects of the exposure to electromagnetic radiation. He was from 2007-2012 a Post-Doctoral Fellow of the FWO-V (Research Foundation - Flanders). Since October 2009 he is professor in the domain of "Experimental Characterization of wireless communication systems." He is IMEC PI since 2017. His professional interests are electromagnetic field exposure assessment, propagation for wireless communication systems, antennas and calibration. Furthermore, he specializes in wireless performance analysis and Quality of Experience.



Arno Thielens received the M.Sc. and Ph.D degrees in engineering physics from Ghent University, Ghent, Belgium, in 2010 and 2015, respectively. He was a PhD student in the Waves group, at that time known as WiCa, of Ghent University's information technology (INTEC) department from 2010-2015, where his research focused on electromagnetism and personal exposure assessment to radio-frequency electromagnetic fields. He was a post-doctoral fellow in the same group, sponsored by the IWT (Institute for Science and Innovation, Flanders, Belgium) from 2015 - 2017. He obtained an FWO [PEGASUS]² Marie Skłodowska-Curie Fellowship in 2017 funded by the European Union's Horizon 2020 research and innovation programme under the Marie Skłodowska-Curie grant agreement No 665501 with the research Foundation Flanders (FWO). He also received an Honorary Fellowship by the Belgian American Education Foundation (BAEF) in the same year. From 2017-2019, he was a postdoctoral fellow at the Berkeley Wireless Research Center at the University of California, Berkeley, where he worked on the development of the human intranet. In 2018, Dr. Thielens was appointed as part-time professor at Ghent University. Since 2020, he is also a senior-postdoctoral fellow of the FWO. His main research interests include exposure of living organisms to electromagnetic fields and wireless propagation in and around the human body.

Dr. Thielens is the recipient of the Joseph James Morrissey Memorial Award issued by the Bioelectromagnetics Society (BEMS) and the European Bio Electromagnetics Association (EBEA) in June 2013. He received the 2015 International Union of Radio Science (Union Radio-Scientifique Internationale or URSI) young scientist award. He also received the Alessandro Chiabrera Award in 2019, granted by the EBFA. He is the co-recipient of three additional publication and presentation awards granted between 2017-2019.